MICROMETEOROID AND SPACE DEBRIS IMPACTS ON THE SPACE FLYER UNIT, AND HYPERVELOCITY IMPACT CALIBRATION OF ITS MATERIALS

M.J. Neish[1], S.P. Deshpande[1], S. Kibe[1], H. Yano[2], Y. Kitazawa[3], S. Yamamoto[4]

[1] *National Aerospace Laboratory, 7-44-1 Jindaijihigashi-machi, Chofu City, Tokyo 182, Japan*
[2] *Planetary Science Division, Institute of Space and Astronautical Sciences, 3-1-1 Yoshinodai, Sagamihara City, Kanagawa 229, Japan*
[3] *Ishikawajima-Harima Heavy Industries (IHI), 1 Shin Nakahara-cho, Isogoku, Yokohama City, Kanagawa 235, Japan*
[4] *Kobe University, Rokkodai-cho, Nada-ku, Kobe 657, Japan*

ABSTRACT

The Space Flyer Unit (SFU) was retrieved by the space shuttle in January 1995, and is presently being subjected to a post-flight analysis with emphasis on the detection and documentation of hypervelocity impact features from space debris and micrometeoroids.

A summary of the analysis procedure is presented here. Some results from preliminary eye surveys are also provided. In addition, more detailed results from high-resolution imaging of craters on two peripheral second-surface mirrors (SSMs) are given, and the morphology of the craters detected in these surfaces is discussed.

First results of hypervelocity impact calibration tests are also included.

1. INTRODUCTION

Japan's Space Flyer Unit (SFU) is a re-usable satellite that was deployed in low-Earth orbit by a H II rocket on 18 March 1995 and retrieved by shuttle STS-72 on 13 January 1996 after 301 days in space. The spacecraft had occupied a circular orbit at an altitude of about 480 km, and an inclination of 28.5°, and had adopted a sun-pointing attitude (i.e., random-tumbling in the geocentric reference frame). It measures 4.46 m in diameter and about 3 m in height. Fig. 1 shows the orbital characteristics and attitude of the SFU with respect to the Earth and Sun, Fig. 2 a photograph taken during the grappling manoeuvre, and Fig. 3 a plan of the SFU satellite itself seen from the -X axis, showing the major experimental surfaces. All surfaces shown here therefore pointed directly into the Sun for the entire mission.

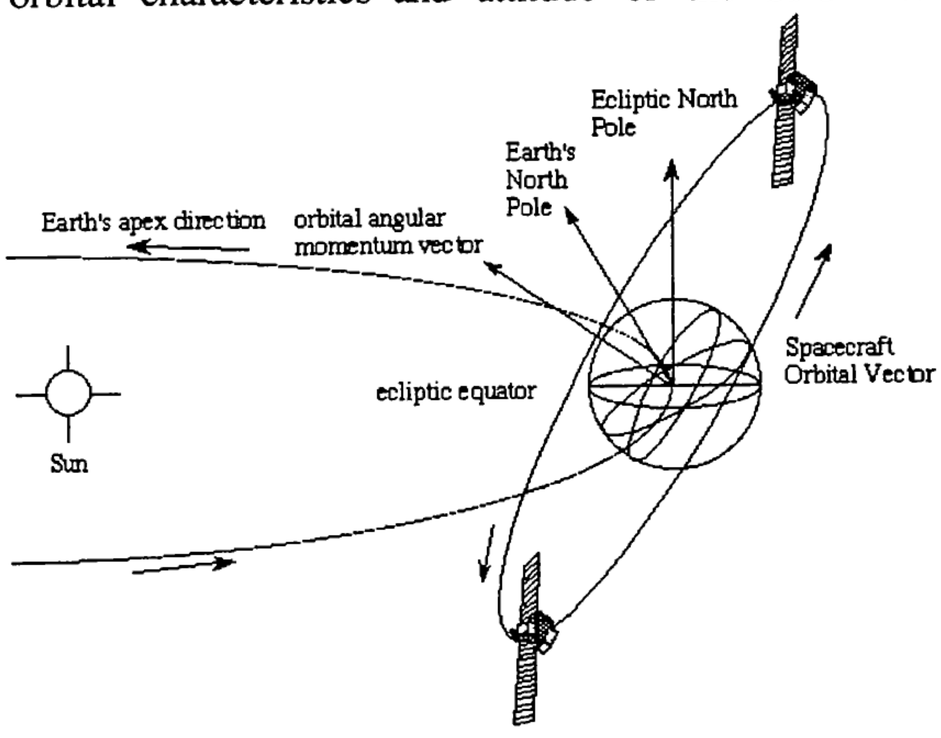

Figure 1: SFU orbital attitude.

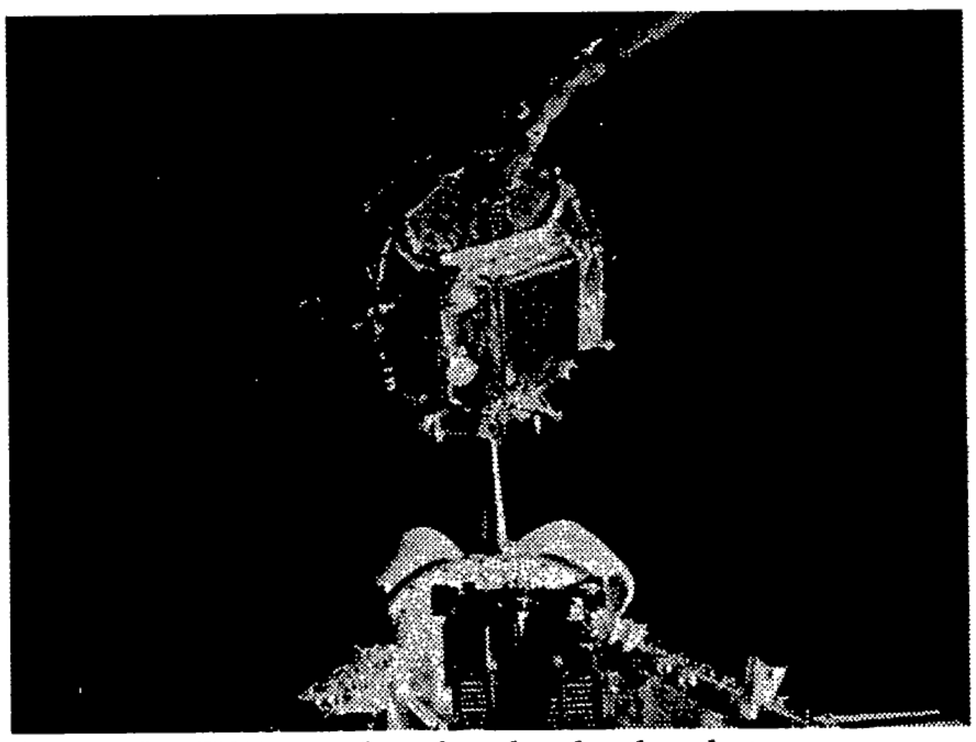

Figure 2: SFU grapple using the shuttle robot arm.

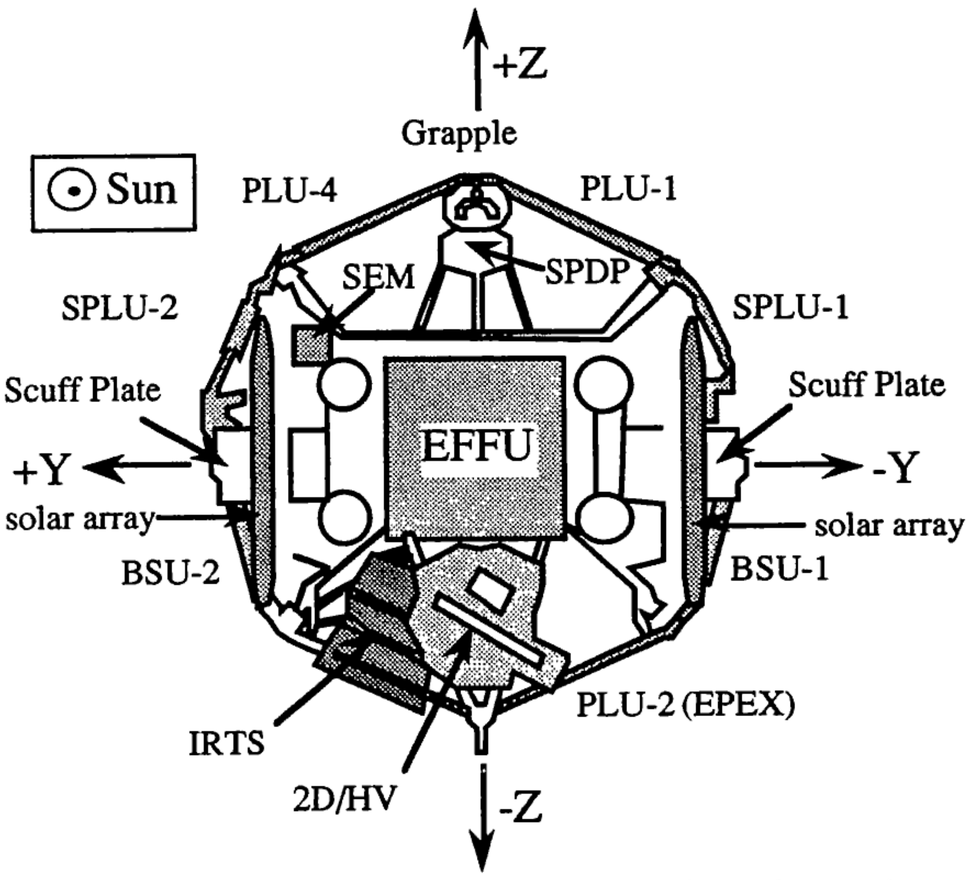

Figure 3: Top view of the SFU showing the various experimental components, the thermal control surfaces of which are the subject of the present post-flight analysis. The view is from the -X direction (from the Sun).

The abbreviations in Fig. 3 stand for the following:

BSU – Bus Unit
EFFU – Exposed Facility Flyer Unit
EPEX – Electric Propulsion Experiment
IRTS – Infra-Red Telescope in Space
PLU – Payload Unit
SPLU – Special Payload Unit
SEM – SFU Environment Monitor
SPDP – Space Plasma Diagnostics Package
2D/HV – Two-Dimensional High Voltage solar array experiment

On retrieval a post-flight investigation programme was immediately commenced, starting at Kennedy Space Center, then moving on to ground operations processing at Astrotech Facility. A contamination assessment and control programme was completed at Astrotech, which indicated that no appreciable contamination had occurred on the spacecraft from either internal payload systems or from the retrieval operation [Ref. 1].

After its arrival in Japan and before de-integration, the SFU underwent a series of visual inspections, down to a minimum diameter of approximately 200 μm. Three particularly large craters were found, the largest one being located on the IRTS, with a diameter of approximately 4.5 mm. More details of the initial surveys are given in Ref. 2.

The total exposed surface area of SFU came to about 150 m^2, two-thirds of which consisted of the solar arrays. Unfortunately these had to be jettisoned during retrieval operations, owing to a failure in the latching mechanism, so the emphasis then shifted to the thermal control surfaces – aluminised Kapton multi-layer insulation (MLI) and silverised Teflon second-surface mirrors (SSM) – as well as the aluminium scuff plates (coated with thermal control paint).

Of all the SFU surfaces, the ones examined in the most detail so far are the peripheral PLU-1 and PLU-4 SSMs, which were situated adjacent to each other on SFU, and were virtually unshielded by any other components (they shall be discussed in Sections 5 and 6). These panels cover an area of 0.94 m^2 each. In addition to these, the IRTS, SPLU-1 and SPLU-2 have been inspected. Owing to the complicated geometry of IRTS it is difficult to extract meaningful flux information from it. As yet no Kapton MLI has been analysed in detail (all the available data are from the preliminary eye surveys). BSU-1 and 2 are not available for scanning. To date, a total of 451 impact craters have been found. A point to note is an unexpected flux ratio of 1.7 between the anti-Sun and Sun-pointing faces [Ref. 2].

Table 1 summarises the number of craters so far discovered, including those found in subsequent higher-resolution scanning (described below).

Surface material	Area examined (m^2)	Nº of impacts observed and imaged
Kapton MLI	10.3	224
Teflon SSM	6.0 (3.0 in detail)	193 (147)
Others	~ 3.0	34 (6)
Total	~ 19.3	451

Table 1: Number of impacts observed on the various SFU surfaces in the preliminary eye inspections and subsequent scanning. In column 3, numbers in brackets represent craters imaged in high detail.

2. SCANNING

After de-integration of SFU the majority of the thermal control surfaces of each major component were delivered to the National Aerospace Laboratory for scanning. Those that could not be delivered were inspected at the owners' site by means of a portable scanning rig. These included SPLU-1, SPLU-2 and IRTS second-surfaces mirrors.

When SSM scanning got under way, it soon became apparent that the eye was much better than a CCD camera at detecting impact features in SSM. This was probably due to the ability of the eye to use specular reflection to distinguish between a depression in the SSM surface and a speck of dust. It was therefore decided to overlay the SSM being examined with a transparent grid of 5 cm x 5 cm squares and to search for impact craters square by square using the naked eye. Potential impact sites were visited with a Keyence zoom lens (magnification 25-175 x) for verification and subsequent digital imaging. This method proved very efficient in terms of time and detection size limit. Human error was kept to a minimum by allowing the observer to take frequent breaks, and by keeping the same observer throughout the scanning.

When an impact crater was identified, it was imaged digitally at the highest magnification which allowed the entire feature to fit within one screen. Higher magnification images were then taken if deemed necessary.

The 25-175 x Keyence lens possessed a very wide depth of focus, and was therefore incapable of selective focussing within the impact craters. In order to take images of the features described in Section 3 below, all features were re-visited using a 150-800 x Keyence zoom lens. Images were taken of the bottom of the holes, the inner Teflon lips (sometimes two were visible in one hole, in which case both were imaged individually) and the outer ring. More images were taken as required if interesting features were discovered in certain holes.

3. SECOND-SURFACE MIRRORS

The structure of second-surface mirrors is obviously a major factor in determining the morphology of its impact craters, discussed in Section 5. The structure for PLU SSM is shown below in Fig. 4, not to scale.

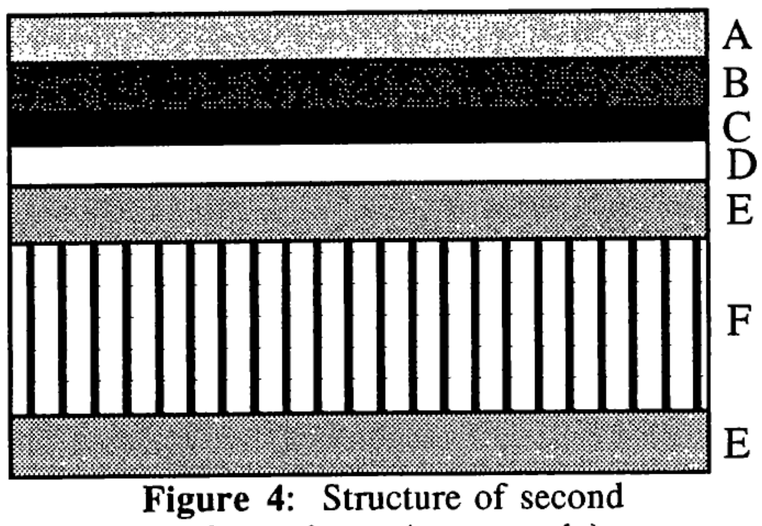

Figure 4: Structure of second surface mirrors (not to scale).

The various layers as labelled in Fig. 4 consist of the following:

A – FEP Teflon tape, thickness, T = 127 μm (= 5 mil.)
B – Silver, T = 1,500 Å
C – Inconel, T = 275 Å
D – 3M 966 acrylic pressure sensitive adhesive, T = 51 μm
E – 2024-T81 aluminium plate, T = 381 μm
F – 5056 aluminium honeycomb, T = 20 mm

A typical impact into SSM material causes the Teflon to come away from the underlying silver paint, creating a circular delamination ring at the point where the Teflon reconnects with the silver (see Fig. 5). Some impact craters, usually the smaller ones, lack this delamination ring altogether. If one examines the central crater, a rough so-called inner Teflon lip is seen at a point above the surface of the SSM. At the bottom of the crater a central pit is often observed, which is in the aluminium in the case of larger impacts, or in the silver layer in the case of the smaller impacts.

As noted by several observers [Refs. 3 and 4] it is not a simple task to define a consistent set of criteria for measuring the various hole dimensions. This is because 1) of the wide diversity of observed impact features, and 2) of the rough texture of the crater walls caused by plastic deformation of the Teflon. Nevertheless, four distinct measurement parameters were defined, as shown in Fig. 5, where the symbols represent the following:

D_m = delamination ring diameter
D_r = ring diameter
D_c = inner Teflon lip diameter
D_p = pit diameter

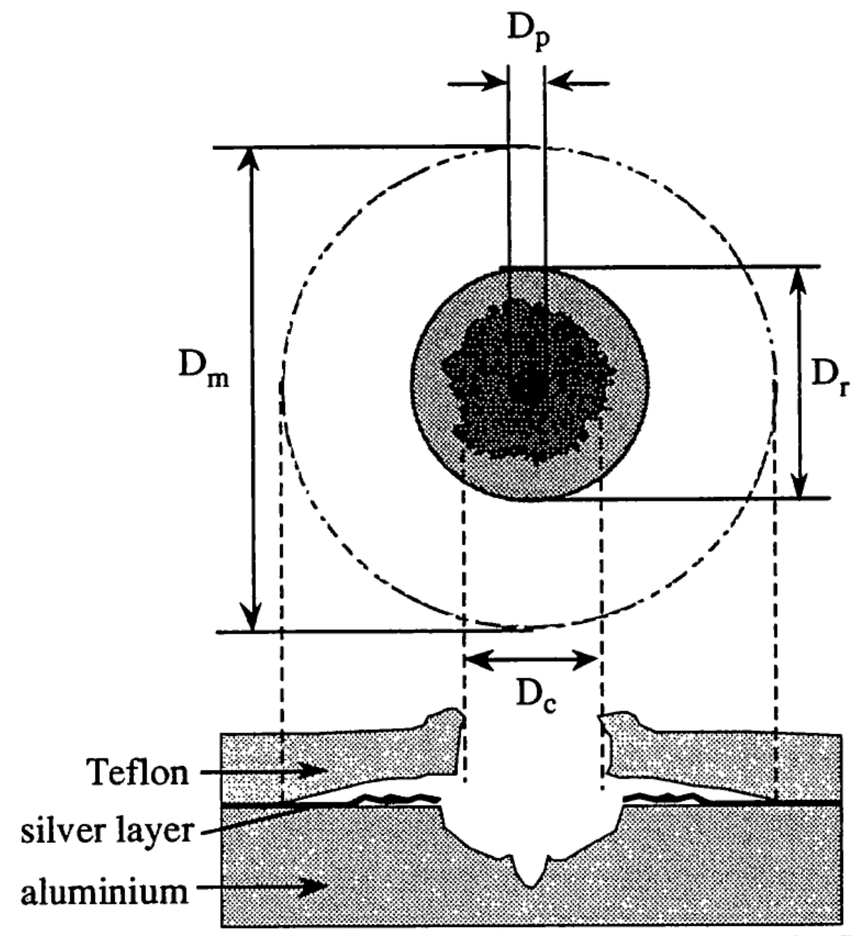

Figure 5: Schematic diagram of a typical impact in SSM material.

4. MEASUREMENTS

Measurement of crater sizes immediately presented a problem owing to the irregular shape of most of the features. Fig. 6 is a close up of one such impact into SSM material, showing clearly the upper Teflon lip visible in the larger features. The measurement problem has been encountered before in other tests using FEP Teflon [Ref. 5].

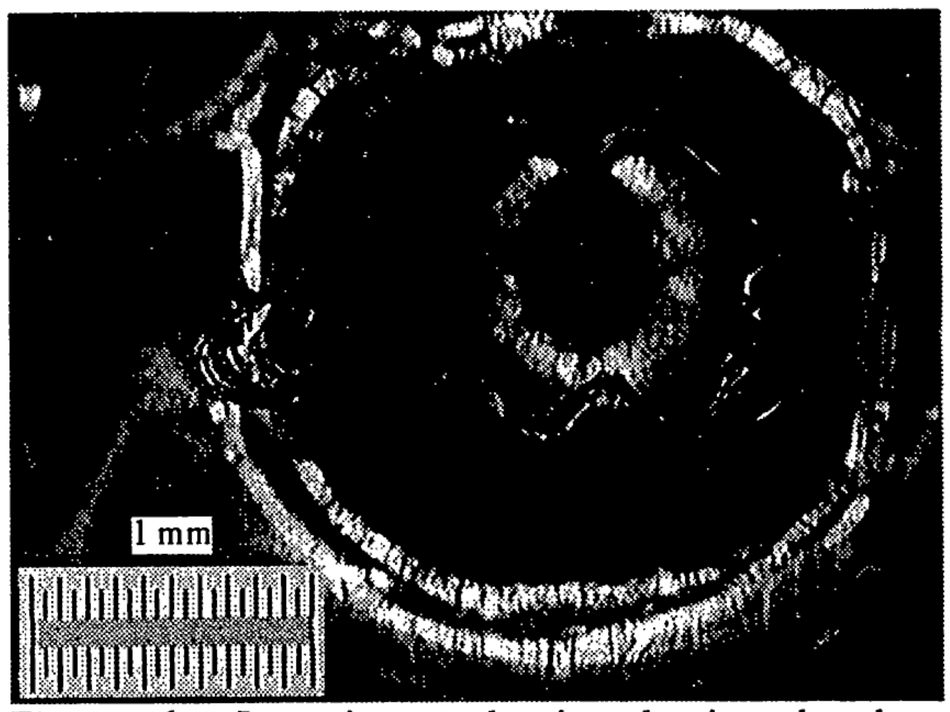

Figure 6: Large impact showing the irregular, but smooth Teflon lip. The diameter is taken as the area enclosed by the lip converted to a circle of equivalent area. Impact is on SPLU-1 second-surface mirror (anti-sun pointing), cell C8.

This was overcome by using the shareware application NIH Image to trace the edge of the lips manually on screen and count the number of pixels lying within the traced line. This was then converted to an equivalent circle covering the same area, the diameter of which was then taken as the diameter of the feature. Although rather time-consuming and labour intensive, this method

gave consistently good results, and could handle the more irregular features which would have been quite impossible to measure by simply taking linear dimensions.

5. MORPHOLOGY

Despite the diversity of observed features on the SSM surfaces, all impact craters could be divided into four so-called "types", named A, B, C and D, the characteristics of each being the following:

A – No visible delamination ring; one Teflon inner lip; central pit usually seen; D_c size range = 44–81 μm

B – Delamination ring; *one* Teflon inner lip; central pit usually visible; looks identical to Type **A** except for the delamination ring; ; D_c size range = 86–176 μm

C – Delamination ring; *two* Teflon inner lips; in many cases extensive damage is seen to the underlying silver layer; D_c size range = 186–413 μm; browning of the silver layer is also visible, in the form of a concentric ring

D – Delamination ring; *no* Teflon inner lip; smooth Teflon *upper* lip, analogous to the crater rim observed in metallic targets, but with a different shape and texture; D_c size range = 564–1641 μm

Examples of the four types are shown in Figs. 7a to 7d.

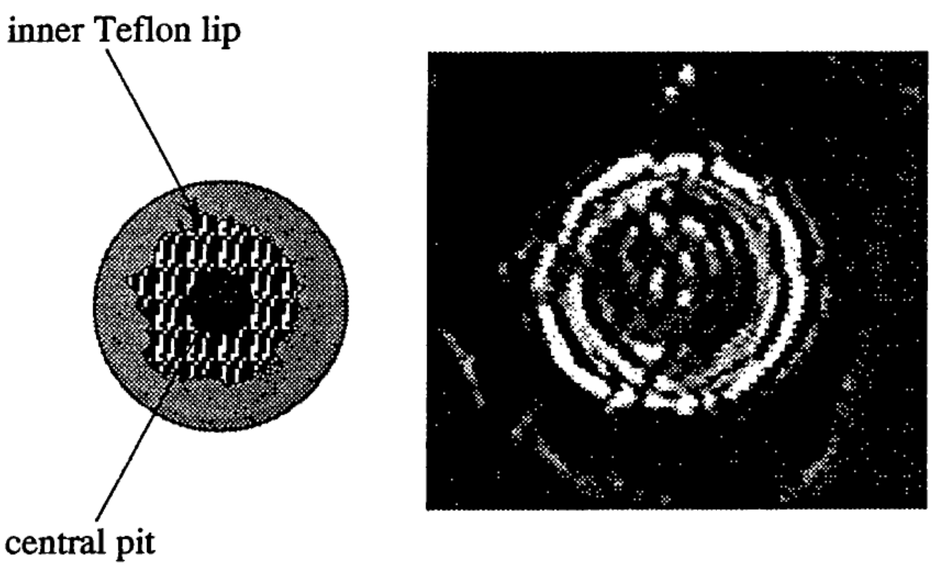

Figure 7a: Type **A** crater (impact K12 on PLU-1)

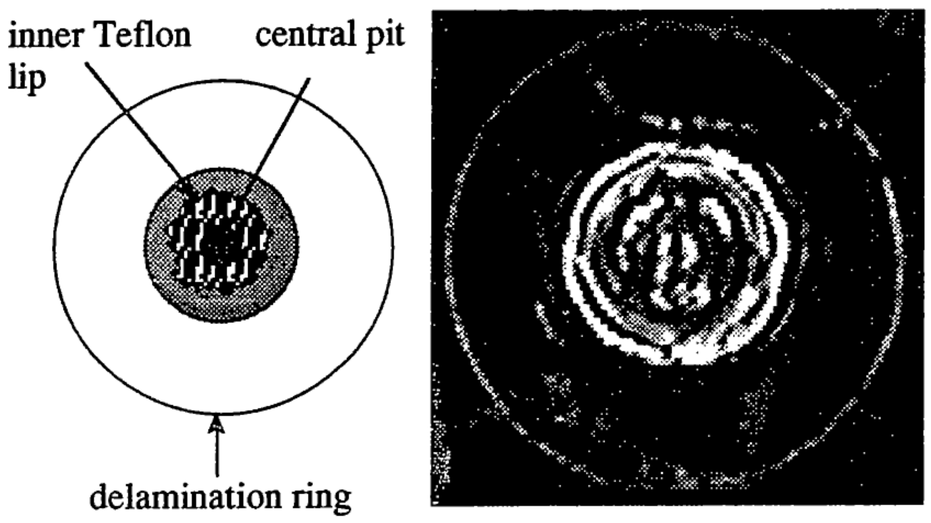

Figure 7b: Type **B** crater (impact P14 on PLU-1)

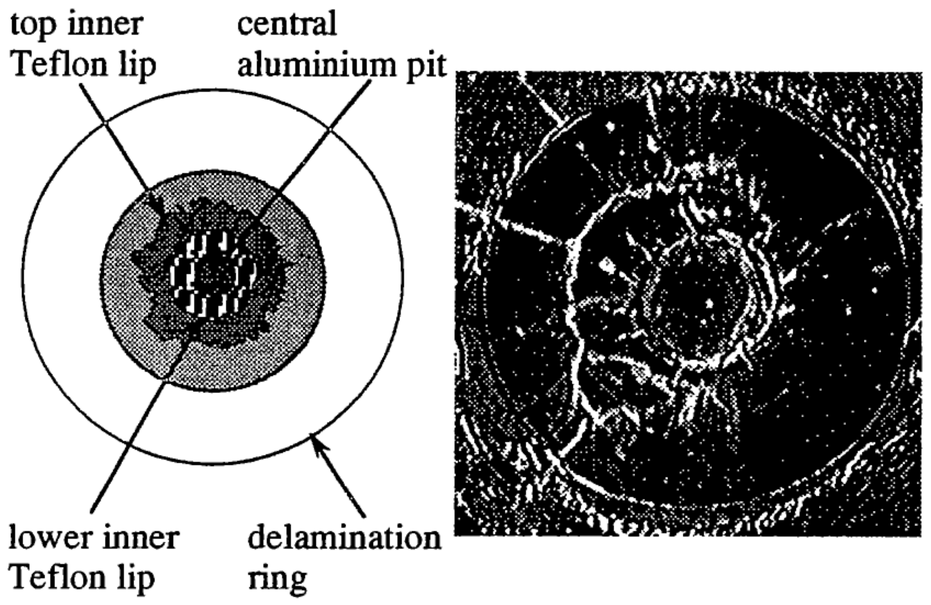

Figure 7c: Type **C** crater (impact O2 on PLU-1)

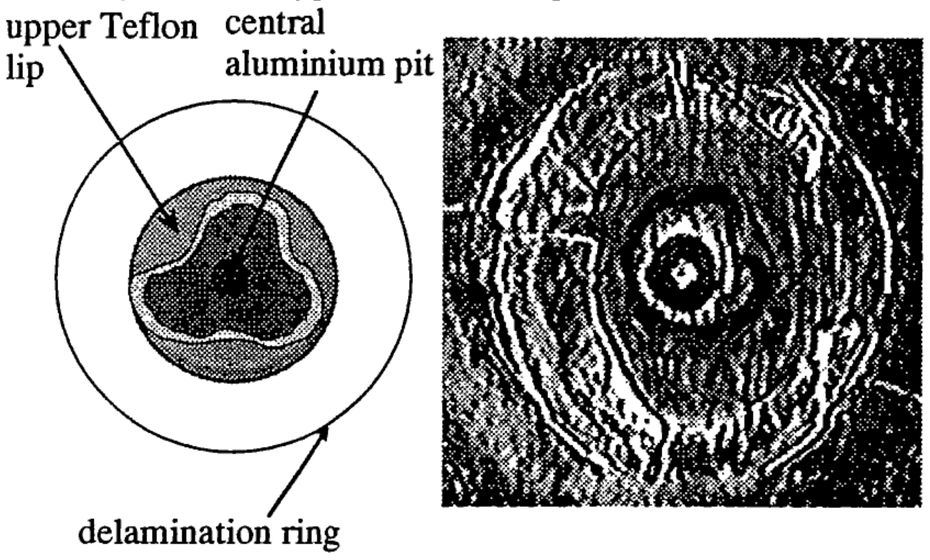

Figure 7d: Type **D** crater (impact I15 on PLU-1)

A break-down of each morphology type is shown in Table 2 for both PLU-1 and PLU-4.

	Nº of impacts of each morphology type			
	Type A	Type B	Type C	Type D
PLU-1	14 (23%)	28 (47.5%)	13 (21.3%)	5 (8.2%)
PLU-4	3 (5.7%)	36 (67.9%)	10 (18.9%)	4 (7.5%)

Table 2: Break-down of each morphology type identified on PLU-1 and PLU-4.

A physical explanation for the occurrence of these morphology types could be used to complement the impact calibration tests. In particular, determining which morphological features are a function of velocity or density, and not of projectile size will assist in the identification of debris or micrometeoroid impacts.

It must be noted that there are a few exceptions to the morphology types describes above. For instance, low velocity hits have no central pit because the impactor did not perforate the top Teflon layer completely.

6. FLUXES

Fig. 8 shows flux as a function of inner Teflon lip diameter for both PLU-1 and PLU-4, assuming an exposure time of 2.6×10^7 seconds. For comparison, the flux for the Long Duration Exposure Facility in terms of crater diameter in semi-infinite aluminium (converted to a random-tumbling plate) is given. Note

that the largest craters did not possess an inner Teflon lip – for these cases the diameter of the top Teflon lip has been plotted. This example highlights the measurement problem described in Section 4: it is not possible to define a morphological feature which is found in all craters, from the smallest to the largest. Other flux curves are available in terms of the other crater measurement parameters – D_m, D_c, and D_p – but are not provided here for space considerations.

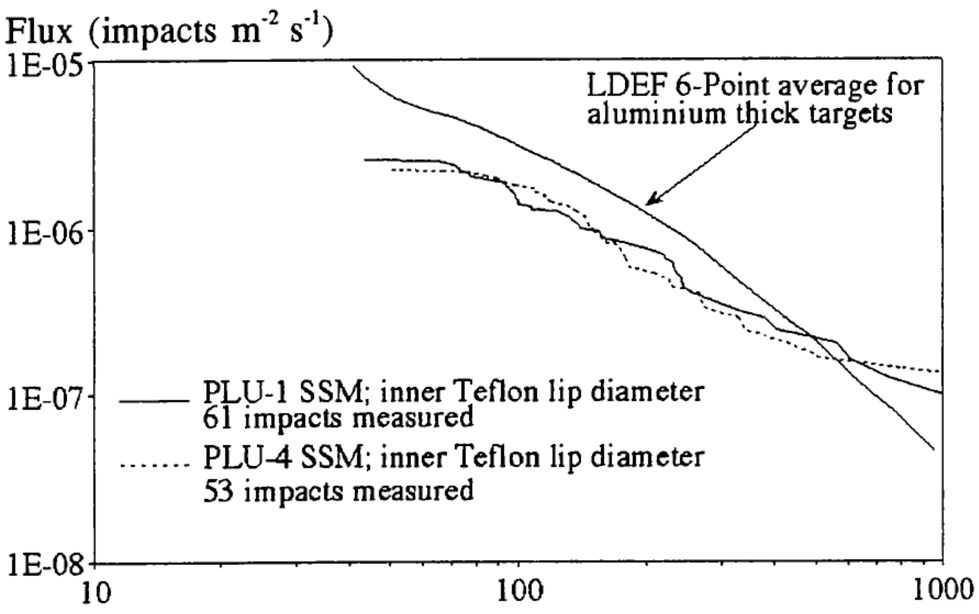

Figure 8: Flux plots for PLU-1 and PLU-4 as a function of inner Teflon lip diameter. These are compared to the LDEF flux as a function of *aluminium foil thickness* penetrated, and converted to a random tumbling plate.

7. CALIBRATION

In order to enable the extraction of particle parameters from the data, a series of impact tests into both Kapton and Teflon have been planned, some of which have already been conducted. The results will be used to derive an empirical equation describing hole or crater size as a function of particle parameters such as mass, velocity and size.

MLI is composed of twelve layers of aluminised Kapton. Although the structure is complicated, since scanning will concentrate only on locating perforations through the top layer (thickness 50 μm) then impact tests into one solitary Kapton film are all that is required.

Using the light gas gun at the University of Kent, a series of impact tests around 5 km s^{-1} were carried out using high-grade glass projectiles (diameter 57-400 μm) onto thin Kapton films of various thicknesses, ranging from 25-175 μm. The rationale behind the tests was to obtain a contour of d/T as a function of D_h /T, where d is the projectile diameter, D_h is the perforation hole diameter and T is the Kapton film thickness. Because of the limited availability of commercial film thicknesses, it was necessary to conduct "shotgun" tests using large numbers of small glass projectiles mounted inside a sabot. This, however, allowed four different film thicknesses to be tested simultaneously, by placing four strips side-by-side on the target plate, as shown in Fig. 9.

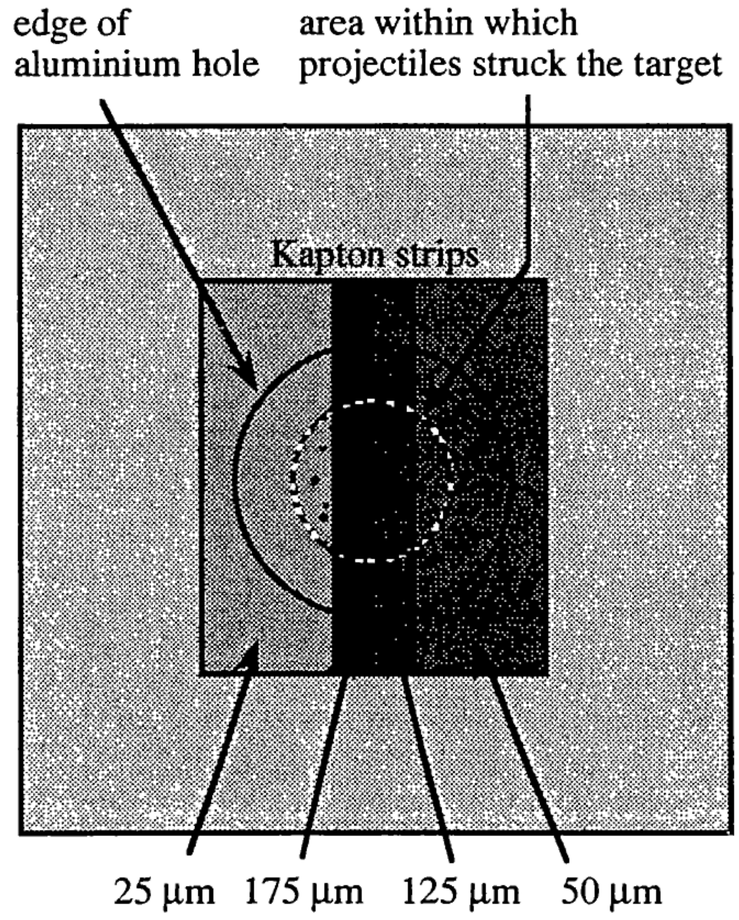

Figure 9: Diagram showing the target configuration used for the calibration shots into Kapton film.

All projectile/film thickness combinations resulted in complete perforations of the target. A summary of the shots is given below in Table 3.

Shot number	Projectile diameter	Target thicknesses	Velocity (km s^{-1})
Test	–	25, 50, 125, 175	4.97
1	57 μm	50, 75, 125, 175	~ 5
2	100 μm	25, 50, 75, 125	failure
3	300 μm	25, 50, 125, 175	~ 5
4	400 μm	25, 50, 75, 125	5.09
2A	100 μm	25, 50, 75, 125	4.85

Table 3: Details of the light gas gun shots into Kapton film.

The resulting perforation holes were then imaged digitally and measured on screen. Owing to the small size of the glass projectiles, there had been some concern before the calibration shots that contaminants of comparable size within the gas-gun launch tube would also perforate the Kapton samples and hide the genuine perforation holes. In the event, this proved to be unfounded, since little scatter was observed in the actual hole diameters. This allowed easy identification of the genuine perforations, and suggested both that there was negligible spread in the projectile diameter and in the velocity distribution.

The results are plotted below in Fig. 10. Included in the figure is a data point on the far right for 7.5-μm Kapton using 100 μm glass projectiles – this was an extra shot done by including a secondary Kapton sample with some primary aerogel samples in a separate experiment. Fig. 10 also shows a curve drawn by hand showing what the

final contour might look like (it is not intended to be a prediction). Note that the marginal perforation regime has not been covered by this particular series of experiments. This means that more tests with a lower d/T ratio must be carried out at the same velocity before more tests are conducted at a higher velocity.

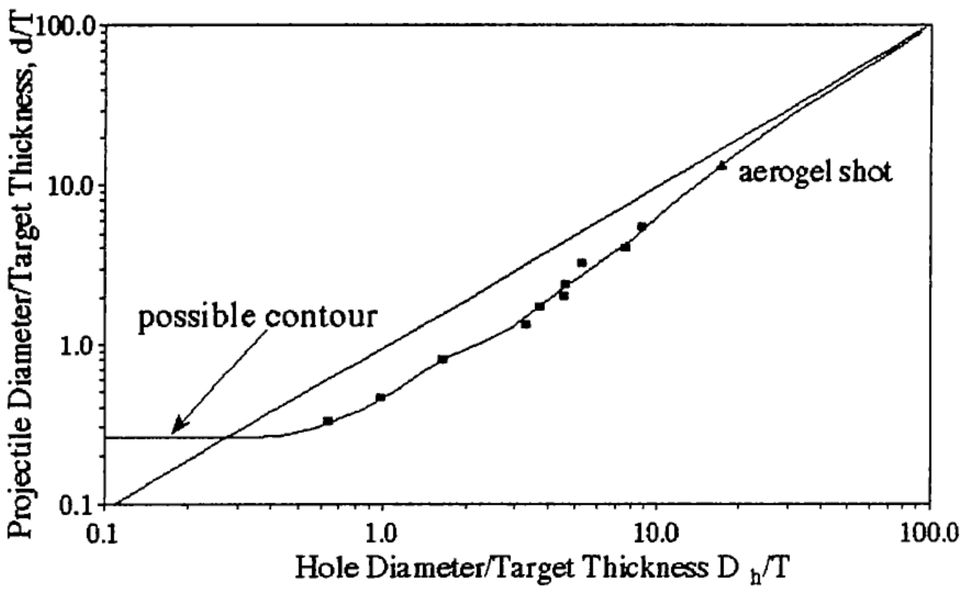

Figure 10: d/T versus D_h/T for the Kapton impact tests.

8. FURTHER WORK

• Further impact tests are planned in the future using a light gas gun or a Van der Graaff accelerator. The hydrocode program AUTODYN-2D™ will be used to complement the results. At first material models in the hydrocode will be refined by means of the laboratory test results; once these are satisfactory, the program will be used to extrapolate to higher velocities.

• A number of representative impact features will be re-examined using a laser microscope in order to extract crater profiles and depths. This will assist in obtaining a physical understanding of how the impact features form, and perhaps allow velocity or density dependent morphological features to be recognised.

• The effect of the space environment, particularly solar VUV radiation from the Sun, on the physical properties of Teflon and Kapton is a phenomenon that needs to be investigated. In material tests described in Refs. 6 and 7, the mechanical properties of Teflon were found to change during and after exposure to simulated solar VUV radiation (the main solar VUV frequency is 121.57 nm, corresponding to the hydrogen Lyman-alpha line). Although no hypervelocity impact tests were carried out by these investigators, it is conceivable that such basic parameters as impact hole size will vary greatly depending on the total dosage of radiation received. This would add a further dimension to the problem of extracting particle parameters from the impact hole size and morphology.

This phenomenon is particularly relevant in the case of EFFU SSM, which comprised a large surface area and received a constant flux of solar VUV radiation for the entire mission.

• After scanning of all surfaces has been completed, extensive chemical analysis of impactor residues will be undertaken.

• Flux results will be compared with those of past missions, such as the Long Duration Exposure Facility (LDEF), European Retrievable Carrier (EuReCa) and the Hubble Space Telescope solar arrays (HST). As the surface materials of all these spacecraft vary widely, a successful comparison will of course depend on accurate hypervelocity impact calibration.

• After completion of data gathering and interpretation it is the authors' intention to compile a database containing our findings and release it to the public via the World Wide Web.

9. REFERENCES

[1] Deshpande, S.P., Maag, C.R., Kibe, S., Neish, M.J., Yano, H. (1997). "Post-Flight Contamination Assessment/Control of the SFU Spacecraft" Presented at the *47th International Astronautical Congress*, Beijing, China, 7-11 October 1996. *IAF-96-I.5.09 to be published in Acta Astronomica.*

[2] Kuriki, K., Takei, M., Wakasugi, N., Yasaka, T. (1996). "Preliminary Results and Further Directions of SFU Post Flight Analysis Activities — Japan's First Investigation of a Retrieved Spacecraft from Space", *Institute of Space and Astronautical Sciences Report Nº 666,* Sagamihara, Tokyo, February 1997.

[3] See, T., Allbrooks, M., Atkinson, D., Simon, C., Zolensky, M. (1990). "Meteoroid and Debris Impact Features Documented on the Long Duration Exposure Facility: A Preliminary Report", *Publication #84, JSC #24608, Space and Life Science Directorate*, Solar System Exploration Branch, NASA Johnson Space Center, Houston, U.S.A.

[4] Mullen, S., McDonnell, J.A.M. (1994). "LDEF LEO Particulate Environment Characterisation", *ESA Contract No. 110745*, ESA/ESTEC, Noordwijk, the Netherlands.

[5] Hörz, F., Cintala, M.J., Bernhard, R.P., See, T.H. (1995). "Cratering and Penetration Experiments in Teflon Targets at Velocities from 1 to 7 km/s", *Int. J. Impact Engng.*, Vol. 17, pp. 419-430, Elsevier Science Ltd, 0734-743X/95.

[6] van Eesbeck, M., Levadou, F., Tupikov, V.I., Cherniavsky, A.I., Khatipov, S.A., Milinchuk, V.K., Stepanov, V.F., "Degradation of Teflon PTFE and FEP to Far Ultraviolet Radiation", *Sixth International Symposium on Materials in a Space Environment*, ESA SP-368, pp. 149-164 (1994).

[7] van Eesbeck, M., Levadou, F., Skurat, V.E., Dorofeev, Y.I., Vasilets, V.N., Barbashev, E.A., "Degradation of Teflon FEP due to VUV and Atomic Oxygen Exposure", *Sixth International Symposium on Materials in a Space Environment*, ESA SP-368, pp. 165-173 (1994).